semiconductor or electro-optic emitters the plasma emitter shows no saturation effects within the examined range of pulse energies of up to 400 μJ. We believe therefore, that the plasma emitter has the potential to become the THz source of choice for ultrahigh-power laser systems (such as 10-Hz, 1-J class of lasers).

1. T. Löffler, F. Jacob, and H.G. Roskos, Appl. Phys. Lett. 77, 453 (2000).
2. Z.G. Lu, P. Campbell, and X.-C. Zhang, Appl. Phys. Lett. 71, 593 (1997).

CThL6 **1:00 pm**

Reflective geometry THz imaging

J.O'Hara, R.A. Cheville, D. Grischkowsky,
Department of Electrical and Computer Engineering and Center for Laser and Photonics Research, 202 Engineering South, Oklahoma State University, Stillwater, OK 74078;
Email: ohara@thzsun.ecen.okstate.edu

Imaging experiments using free-space pulses of terahertz (THz) radiation have been demonstrated.[1] Traditionally THz imaging systems generate images via transmission measurements. But imaging can be done in a reflection geometry where the THz beam illuminates the target and its reflections are collected and measured. Unlike others, this method allows the measurement of non-uniform, opaque objects.

The THz imaging system is similar to previous THz impulse ranging systems[2] up to the target. Beyond the target the systems differ. As shown in Figure 1, the target's scattered energy is collected by a 6 inch diameter spherical mirror with a focal length of 12 inches. This mirror focuses the collected radiation back to the receiver. The mirror is placed 24 inches from both the target and the receiver to achieve one-to-one imaging of the target onto the receiver.

With the image at the receiver, the time delay is scanned to form a time-domain measurement of the image at that point. Incremental target movements, in the x-direction, between successive time scans form a 2D image of the target. An example of an image is shown in Figure 2. Imaging in 3D simply requires additional target movements in the vertical or y-direction. Figure 2 clearly demonstrates the dual nature of the system; namely that it simultaneously produces both temporally resolved and spatially (diffraction-limited) resolved images. This unveils one of the most distinct features of the THz image: the sharp contrast between the resolution in the temporal dimension and the resolution in the spatial dimension. To validate using the term "2D" it is important to note that the temporal dimension (in ps) can be directly translated to the z-axis spatial dimension (in mm) by multiplying by 0.3.

In the temporal dimension, it is appropriate to adopt the concept of range resolution. With a main pulse width of approximately $\tau = 800$ fs, the radar ranging formula $\Delta R = c\,\tau/2$ yields a resolution of $\Delta R = 120$ μm. Unlike the temporal dimension, the spatial dimension is independent of the phase information contained in the pulse and consequently cannot take advantage of the phase coherence to improve its resolution.

Hence, for the spatial dimension, a different approach is necessary. Since the target is a very small sphere, it can be approximated that its scattered radiation reaching the collection mirror is essentially a spherical wave radiated from a point source. The imaging system smears out this point source feature by diffraction where the spherical mirror acts as a circular aperture. The diffraction limits the distinguishable feature size and, as long as the target is sufficiently smaller than the measured pixel, this diffracted size determines the system's amplitude pixel size. For the frequency range of this THz imaging system, the amplitude pixel size (full-width-half-max) ranges from 2 mm up. This is significantly larger than the target diameter of 1 mm so that this pixel size is determined by the imaging system and not by the target. The pixel diameter defines the system resolution so, given a complex target, it should be possible to predict the resulting image based on this pixel size.

Like the time-domain information, the spectral information can be extracted from the data using the discrete Fourier transform method on

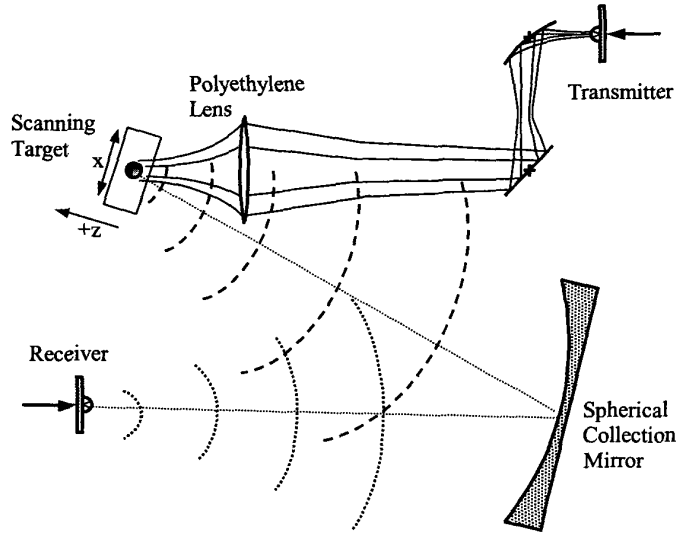

CThL6 Fig. 1. THz imaging system layout. The target, a 1 mm steel ball, is placed atop a fin-shaped (for stealth purposes) paraffin holder and is translated in the x-direction via a motorized scanning stage.

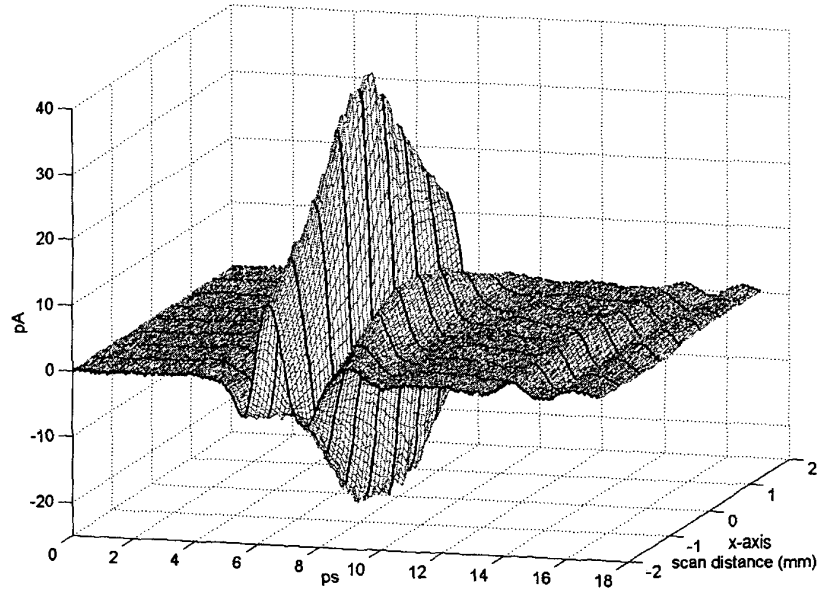

CThL6 Fig. 2. Two-dimensional image of target. The image has one temporal and one spatial dimension corresponding to the differing range and spatial resolutions of the system. The temporal dimension (in ps) can be directly translated to the z-axis spatial dimension (in mm) by multiplying by 0.3. Darker lines are drawn for clarity.

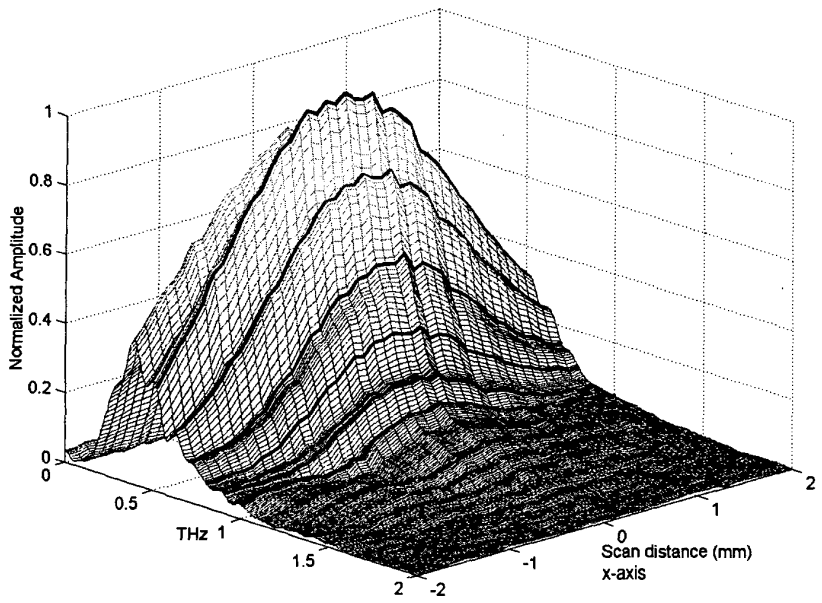

CThL6 Fig. 3. Experimental spectra obtained from THz image data. Darkened curves show individual frequency's spatial distributions or pixel sizes.

the individual scans. As in the time-domain, these plots have two different axes: the spatial and spectral axes. This data can be used to show the continuous effect of wavelength on spot (pixel) size. As expected, given the fixed aperture size, the higher frequency components show a decrease in spot size. Equivalently, the image becomes sharper with increased frequency. Figure 3 shows the experimental spectra obtained from the data used to generate Figure 2, with useful spectra bounded between 0.2 THz and 2 THz.

Reflective THz imaging promises application in non-invasive arenas where microwave and optical techniques cannot be used. Applications such as burn diagnostics and near-surface tomography could benefit greatly from such an arrangement.[1]

References

1. D. Mittleman, R. Jacobsen, and M. Nuss, "T-Ray Imaging", *IEEE J. Selected Topics Quantum Electron.* **2**, 679–692 (1996).
2. R.A. Cheville and D. Grischkowsky, "Time domain terahertz impulse ranging studies," *Appl. Phys. Lett.* **67**, 1960–1962 (1995).

CThL7 **1:00 pm**

Electron and atomic force microscopy studies of femtosecond laser machining of Si, GaAs and InP

A. Borowiec, M. MacKenzie, G.C. Weatherly, H.K. Haugen, *Brockhouse Institute for Materials Research, McMaster University, Hamilton, Ontario, Canada L8S 4M1; Email: borowia@mcmaster.ca*

The application of femtosecond light pulses to materials processing has recently become a topic of great interest.[1] Femtosecond laser ablation dynamics has been extensively studied by techniques including time-of-flight and has also been treated theoretically [see, e.g., 2–4]. However, although numerous experimental studies have demonstrated excellent spatial control in femtosecond laser machining, relatively few investigations have explored details of the near-surface changes in crystallographic structure and the localized changes in target composition. In this study we characterize laser-machined semiconductor samples, employing a combination of scanning (SEM) and transmission (TEM) electron microscopies as well as atomic force microscopy (AFM).

Laser pulses of 120 fs duration are obtained from an amplified Ti:sapphire laser with a wavelength ≈788 nm. The laser is focused on the sample by a 10× microscope objective to a spot size of 6 μm ($2w_0$ at $1/e^2$). A small vacuum chamber mounted on a computer-controlled xyz translation stage was used for target processing. Typically, single laser shots on pristine sample surfaces are employed. Studies on crater morphology are conducted for a wide range of pulse energies extending to a maximum ≈2 μJ.

Figure 1 shows analyses of single laser shot irradiation of Si, GaAs and InP. In our case, the damage thresholds for Si, GaAs and InP are 25 ± 5 nJ, 16 ± 5 nJ and 10 ± 5 nJ respectively. The crater geometries are very reproducible in the lower pulse energy regime, with Si leading to the most pronounced rims around the outer edge.

For lower pulse energies (limited to approximately 400 nJ in Si and GaAs, and to 200 nJ in InP), our TEM investigations reveal very different crystallographic structures for the residual material near the laser-ablated regions in the three semiconductors. For example, the Si craters appear to remain single crystal with evidence for polycrystalline material in the pronounced rims of the craters; whereas in the case of InP, 5–30 nm polycrystalline grains were found over the ablated surfaces as well as in the outer rims of the craters. An example of the TEM analysis of InP is shown in Fig. 2.

We gratefully acknowledge the support of MMO and NSERC.

1. See, e.g., S. Nolte et al, Opt. Lett. **24**, 914 (1999); X. Liu, D. Du, and G. Mourou, IEEE J. Quantum Electron. **33**, 1706 (1997); T. Juhasz et al, in Ultrafast Phenomena XI, p. 687 (1998).
2. A. Cavalleri et al, J. Appl. Phys. **85**, 3301 (1999); K. Sokolowski-Tintin et al, Phys. Rev. **B58**, R11805 (1998).
3. R.F.W. Herrmann et al, Appl. Phys. A **66**, 35 (1998).
4. S.I. Anisimov et al, Appl. Phys. A **69**, 617 (1999); N.A. Inogamov et al, JETP Lett. **69**, 310 (1999).

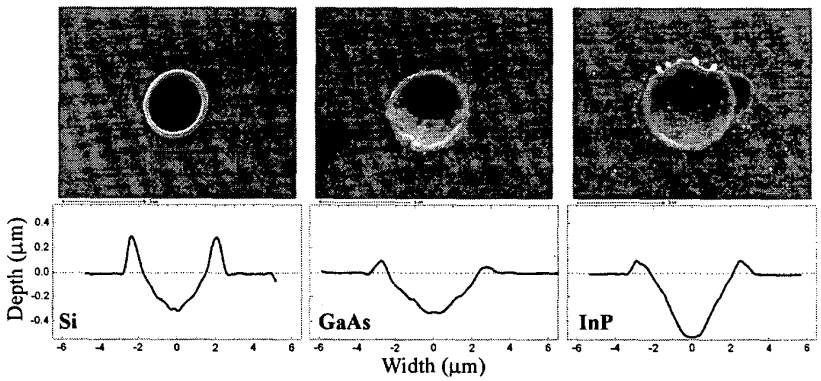

CThL7 Fig. 1. SEM images and corresponding AFM scans for (a) 160 nJ pulse on Si, (b) 130 nJ on GaAs, and (c) 145 nJ on InP. The dashed line indicates the position of the surface prior to irradiation.